Efficient Degradation of Methylene Blue Using La-PTC-HIna/$Ti_3C_2T_x$ MXene: Adsorption and Photocatalytic Degradation

Agustino Zulys[1*], Adawiah Adawiah[2], and Nasruddin Nasruddin[3]

[1]*Department of Chemistry, Faculty of Mathematics and Natural Sciences, Universitas Indonesia, Depok, 16424, Indonesia*

[2]*Integrated Laboratory Centre, Faculty of Science and Technology, UIN Syarif Hidayatullah Jakarta, Jl. Ir. H. Juanda No. 95, Ciputat 15412, Indonesia*

[3]*Department of Mechanical Engineering, Faculty of Engineering, Universitas Indonesia, Depok, 16424, Indonesia*

* ***Corresponding author:***

email: zulys@ui.ac.id

Received: December 29, 2021
Accepted: July 24, 2022

DOI: 10.22146/ijc.71692

Abstract: *Isonicotinic acid is a pyridine carboxylic compound that can be used as a linker to construct coordination complexes. Adding isonicotinic acid (HIna) to the metal-organic framework (MOF) enhanced the MOF surface area, pore volume, and pore size and increased its catalytic activity. $Ti_3C_2T_x$ MXene nanosheet with excellent metal conductivity was also employed on MOF to optimize its functionality. This work aims to synthesize MOF modulated isonicotinic acid La-PTC-HIna and design the new materials: La-PTC/$Ti_3C_2T_x$ MXene and La-PTC-HIna/$Ti_3C_2T_x$ MXene hybrid, then apply them for methylene blue photodegradation. La-PTC-HIna, La-PTC/$Ti_3C_2T_x$ MXene, and La-PTC-HIna/$Ti_3C_2T_x$ MXene were synthesized by the sonochemical method. MOF La-PTC-HIna has the highest methylene blue photocatalytic degradation activity than MOF La-PTC, $Ti_3C_2T_x$ MXene, La-PTC/$Ti_3C_2T_x$ MXene, and La-PTC-HIna/$Ti_3C_2T_x$ MXene with degradation efficiency of 99.48% in 20 ppm methylene blue under visible irradiation for 210 min. This study reveals the La-PTC-HIna and La-PTC-HIna/$Ti_3C_2T_x$ MXene as a new material that has the potential to remove methylene blue from an aqueous solution.*

Keywords: *metal-organic framework; $Ti_3C_2T_x$ MXene; La-PTC; La-PTC-Hina; La-PTC/Ti_3C_2Tx MXene; La-PTC-HIna/Ti_3C_2Tx MXene*

■ INTRODUCTION

The textile industry is one of the primary industrial sectors contributing to water pollution. The textile industry releases about 20% of organic dye waste worldwide [1]. These organic dyes are difficult to degrade, toxic, and disrupt aquatic ecosystems. In the last few decades, many nanomaterials have been used to treat dyes waste, i.e., modified bentonite [2], activated carbon [3], metal-organic frameworks (MOFs) [4], and MXene [5].

MOFs are nanoporous materials that consist of coordination bonds between transition-metal cations and multidentate organic linkers [6]. These materials have unique properties, such as large surface area and porosity [7], abundant active sites, redox ability, tunable structure, and pore size [8]. Therefore, MOFs can be used to eliminate dyes contaminant from water. Several researchers reported MOFs as a nanomaterial for photocatalytic dye degradation. Zulys et al. [9] reported MOFs La-PTC-based sodium perylene-3,4,9,10-tetracarboxylic as an organic linker and lanthanum metal ion. MOFs La-PTC degrade methylene blue at 67.02% for 240 min under visible light irradiation in the presence of hydrogen peroxide 0.2 M.

The photocatalytic activity of MOF was enhanced by adding modulator compounds like isonicotinic acid. Isonicotinic acid is a pyridine carboxylate compound that can be an excellent linker to construct coordination complexes [10]. Garibay et al. [11] reported that the addition of isonicotinic acid increases MOFs' size and pore volume and enhances their catalytic activity. Adawiah et al. [12] also reported that MOFs Cr-PTC-HIna has higher photocatalytic activity than Cr-PTC in methylene blue degradation.

MXene is a new type of two-dimensional (2D) material produced by etching a layer of "A" groups from MAX phases, where M is a transition metal like titanium, A is an IVA/IIA (e.g., H, Al, Ga, In, Si, Ge, Sn, Pb, P, or As), and X is nitrogen or carbon [13]. They are composed of transition metal carbides and nitrides with different functional groups like OH^-, O^-, and F^- attached to their surface. The general chemical formula of MXene is $M_{n+1}X_nT_x$, where M is the transition metal like titanium, X is carbon, and T_x is the termination group like OH^-, O^-, and F^- [14-17]. MXene can be applied for treating dyes wastewater because of its physicochemical properties, including high surface area, chemical stability, hydrophilicity, and structure [18]. Besides, the electrical conductivity of Ti_3C_2 MXene is 4600 ± 1100 $S.cm^{-1}$ with highly anisotropic carrier mobility, favoring the capture and transfer of photogenerated electron-hole pairs in the photocatalysis process [19].

According to previous studies by other researchers, MOFs also are often combined with other materials to protect the MOFs from degradation and enhance their photocatalytic activity. Wang et al. [20] reported the synthesis of Ti_3C_2 MXene/MIL-100(Fe) composite for the photocatalytic oxidation of nitrogen fixation. Tian et al. [21] used $Ti_3C_2/TiO_2/UiO\text{-}66\text{-}NH_2$ hybrids for the photocatalytic reaction of hydrogen gas evolution. Jun et al. [18] reported $Ti_3C_2T_x$ MXene and Al-based metal-organic framework for methylene blue and acid blue 80 adsorptions.

Thus, it is reasonable for us to design new material-based MOFs La-PTC that are modulated by isonicotinic acid (HIna) and combined with $Ti_3C_2T_x$ MXene. This study aims to investigate their characteristics and performance for methylene blue photocatalytic degradation.

■ EXPERIMENTAL SECTION

Materials

All materials were purchased and used without any purification. $La(NO_3)_3{\cdot}6H_2O$ (Merck), dimethyl formamide (DMF) (Merck), sodium hydroxide (Merck), ethanol absolute (Merck), isonicotinic acid (IDN), and $Ti_3C_2T_x$ MXene (Nanochemazone).

Instrumentation

All materials were characterized by X-ray diffraction (PXRD) to determine crystallinity, Fourier transforms infrared (FT-IR) spectroscopy to investigate the functional groups, ultraviolet-visible diffusion reflectance spectroscopy (Shimadzu UV 2700) to measure the band gap, the Brunauer Emmett Teller (BET) surface area analyzer (Micromeritics, ASAP 2020) to evaluate the surface area, pore volume and pore size, and scanning electron microscope energy dispersive X-ray (EDX) spectroscopy to obtain the particle morphology.

Procedure

Preparation of sodium perylene-3,4,9,10-tetracarboxylate (Na_4PTC)

Perylene-3,4,9,10-tetracarboxylic dianhydride (PTCDA) (0.5 g, 1.27 mmol) was dissolved in distilled water (50 mL) on a beaker glass. NaOH (0.356 g, 8.9 mmol) was added to the mixture while stirring vigorously at 300 rpm for 1 h. The greenish-yellow solution was obtained and filtered. Then, excess ethanol was added to obtain a yellow sodium perylene-3,4,9,10-tetracarboxylic (Na_4PTC) precipitate. The yellow bulk powder of Na_4PTC was collected by filtration, washed with ethanol until a pH of 7 was reached, and dried at room temperature overnight.

Synthesis of MOF La-PTC

MOF La-PTC was synthesized according to the method in our previous research [9] $La(NO_3)_3{\cdot}6H_2O$ powder, Na_4PTC at a molar ratio of 1.0:0.5 in dimethyl formamide (DMF), and deionized water mixture (1:5 v/v) in a Teflon liner. After the mixture was stirred magnetically at 300 rpm for 60 min, the Teflon liner was sealed in a solvothermal reactor and heated at 170 °C for 24 h. After cooling to room temperature, the product was purified and washed with deionized water and DMF to remove residual Na_4PTC and other impurities. Finally, the orange powder product was centrifuged and dried at 70 °C overnight.

Synthesis of La-PTC-HIna

$La(NO_3)_3{\cdot}6H_2O$ powder, Na_4PTC, and isonicotinic acid were mixed at a molar ratio of 1.0:0.5:1.0 in DMF

and deionized water mixture (1:5 v/v) in a beaker glass. Then, the mixture was stirred magnetically at 300 rpm for 120 min and ultrasonically treated for 2 h. The bulk powder was filtrated and washed with deionized water and DMF to remove residual Na_4PTC and other impurities. Finally, the brown powder product was centrifuged and dried at 70 °C overnight.

Synthesis of La-PTC/$Ti_3C_2T_x$ MXene

The La-PTC/$Ti_3C_2T_x$ MXene nanocomposites were constructed by a facile synthetic method. MOF La-PTC and quantitative $Ti_3C_2T_x$ MXene (20 wt.%) were put into ethanol absolute. The mixture was stirred for 24 h at 300 rpm, ultrasonically treated for 3 h, and then dried at 60 °C for 18 h. The product was then heated in a 300 °C furnace for 2 h. Finally, the $Ti_3C_2T_x$ MXene nanosheets were coupled with MOF La-PTC after grinding.

Synthesis of La-PTC-HIna/$Ti_3C_2T_x$ MXene

$La(NO_3)_3{\cdot}6H_2O$ powder, Na_4PTC, and isonicotinic acid were mixed at a molar ratio of 1.0:0.5:1.0 in DMF and deionized water mixture (1:5 v/v) in a beaker glass. Then a quantitative Ti_3C_2 MXene (20 wt.%) was added. Then, the mixture was stirred magnetically at 300 rpm for 120 min and ultrasonically treated for 2 h. The precipitate was filtrated and washed with deionized water and DMF to remove residual Na_4PTC and other impurities. Finally, the brown powder product was centrifuged and dried at 70 °C overnight.

Degradation of methylene blue analysis

The material (25 mg) was dispersed in 50 mL of methylene blue (MB) solution (20 ppm) in a Pyrex reactor. Subsequently, the sample was irradiated with the 250 W mercury lamp with stirring at 300 rpm and room temperature. The concentration of MB after the reaction was measured by a UV-Visible spectrophotometer at 665 nm. The methylene blue degradation efficiency is calculated using Eq. (1). A control experiment was carried out under dark condition.

$$DE(\%) = \frac{Co - Ct}{Co} \times 100\% \quad (1)$$

where DE (%) is the degradation efficiency of methylene blue, Co is the initial concentration, and Ct is the final concentration.

■ RESULTS AND DISCUSSION

Characteristic of Photocatalysts

The XRD analysis showed the different diffraction spectrums of materials. Fig. 1 shows that La-PTC-HIna and La-PTC-HIna/$Ti_3C_2T_x$ MXene have amorphous forms, while the other three have pretty good crystallinity. The XRD peaks of La-PTC were observed at 2θ = 6.31°, 12.64°, 16.6°, 28.7°, 33.3°, 44.6°, 47.9°, 50.9°, 59.6°, 62.3°, 70°, 77.3° [9]. Peaks at 2θ = 9.0°, 18.3°, 27.7°, 36.1°, 41.9°, and 60.7° correspond to the (002), (004), (006), (101), (105), and (110) reflections of $Ti_3C_2T_x$ MXene [22]. Peaks at 2θ = 5.7°, 8.4°, 12.1°, 18.5 °, 20.9°, 22.9°, 26.9°, and 29.3° are characteristics of La-PTC/$Ti_3C_2T_x$ MXene (Fig. 1). It shows a chemical interaction between $Ti_3C_2T_x$ MXene and La-PTC compounds which looks at the difference in the spectrum of the three materials. Meanwhile, for La-PTC-HIna and La-PTC-HIna/$Ti_3C_2T_x$ MXene, the spectral peaks cannot be determined because the resulting particles are amorphous.

FT-IR spectroscopy was employed to determine the functional groups in the five materials. The infrared spectrum of all materials can be seen in Fig. 2 and Table 1. The FTIR spectrum of La-PTC/$Ti_3C_2T_x$ Mxene is very similar to La-PTC, and La-PTC-HIna/$Ti_3C_2T_x$ Mxene is

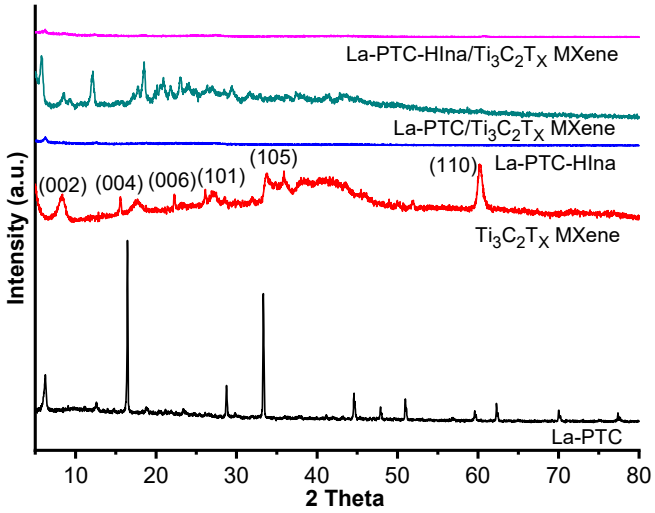

Fig 1. XRD pattern of MOF La-PTC, $Ti_3C_2T_x$ MXene, La-PTC/$Ti_3C_2T_x$ MXene, La-PTC-HIna, and La-PTC-HIna/$Ti_3C_2T_x$ Mxene

Table 1. Wavenumber and functional group of materials

Wavenumber (cm^{-1})					Description
$Ti_3C_2T_x$ MXene	La-PTC	La-PTC-HIna	La-PTC/$Ti_3C_2T_x$ MXene	La-PTC-HIna/$Ti_3C_2T_x$ MXene	
425			421	424	the deformation vibration of the Ti–O bond
506			501	502	Ti-C vibration
	572	570	556	568	La-O vibration
	749	759	761	757	Out of plane C=C aromatic ring
	849, 808	849, 807	848, 807	858, 807	Bending vibration (C-H) out of plane aromatic ring
	1210	1207	1209	1233	Bending vibration (C-H) in plane aromatic ring
	1530	1585	1590	1591	asymmetric stretching vibration (-COO)
	1434	1526	1503	1537	symmetric stretching vibration (-COO)
3034		3356	3399	3117	Hydroxyl (OH)

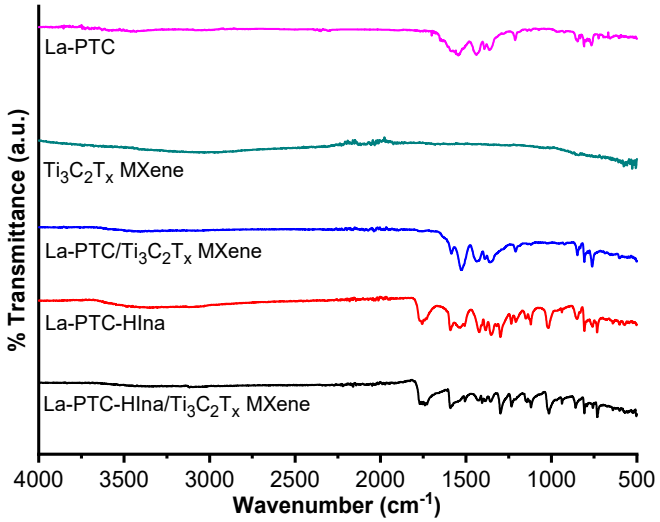

Fig 2. IR spectrum of MOF La-PTC, $Ti_3C_2T_x$ MXene, La-PTC/$Ti_3C_2T_x$ MXene, La-PTC-HIna, and La-PTC-HIna/$Ti_3C_2T_x$ MXene

very similar to La-PTC-HIna. It indicates the functional group consistency of the La-PTC and La-PTC-HIna materials on the surface of the La-PTC/$Ti_3C_2T_x$ Mxene and La-PTC-HIna/$Ti_3C_2T_x$ Mxene hybrid.

A UV-Vis spectrophotometer was carried out to determine the band gap energy and visible light absorption capacity of the materials. Fig. 3 exhibits the absorption band edges for the La-PTC, $Ti_3C_2T_x$ MXene, La-PTC-HIna, La-PTC/$Ti_3C_2T_x$ MXene, and La-PTC-HIna/$Ti_3C_2T_x$ MXene composite. The band gap energy of those materials was calculated using the Kubelka-Munk equation ($\alpha h\nu = A(h\nu\ Eg)^2$) [23]. The calculation results in the band gap energy of $Ti_3C_2T_x$ MXene of 1.3 eV (Table 2) and does not show an absorption band because it is a metallic material [24]. La-PTC/$Ti_3C_2T_x$ MXene hybrid band gap (2.3 eV) is higher than that of the La-PTC (2.21 eV). In contrast, the band gap energy of La-PTC-HIna/$Ti_3C_2T_x$ MXene composite (1.9 eV) is less than La-PTC-HIna (2.02 eV). It confirmed that the Ti, C, and O doping process from $Ti_3C_2T_x$ MXene to the surface of the La-PTC and La-PTC-HIna structure had been successfully carried out. This difference occurs because of the heterojunction formed by MOF La-PTC, La-PTC-HIna, and $Ti_3C_2T_x$ MXene, forming a new material. On the other hand, the band gap energy of La-PTC-HIna (2.02 eV) is less than La-PTC. (2.2 eV) The factor that can affect the bandgap energy is particle size. Modulated isonicotinic acid in the La-PTC reduces its particle size. The decreased particle size generated the MOFs charge carriers to interact quantum mechanically. It leads to a discrete electrolytic state which increases bandgap energy and a shift in band edge.

Table 2. Band gap energy of materials

Material	E_g (eV)
$Ti_3C_2T_x$ MXene	1.30
La-PTC	2.20
La-PTC-HIna	2.02
La-PTC/$Ti_3C_2T_x$ MXene	2.30
La-PTC-HIna/$Ti_3C_2T_x$ MXene	1.90

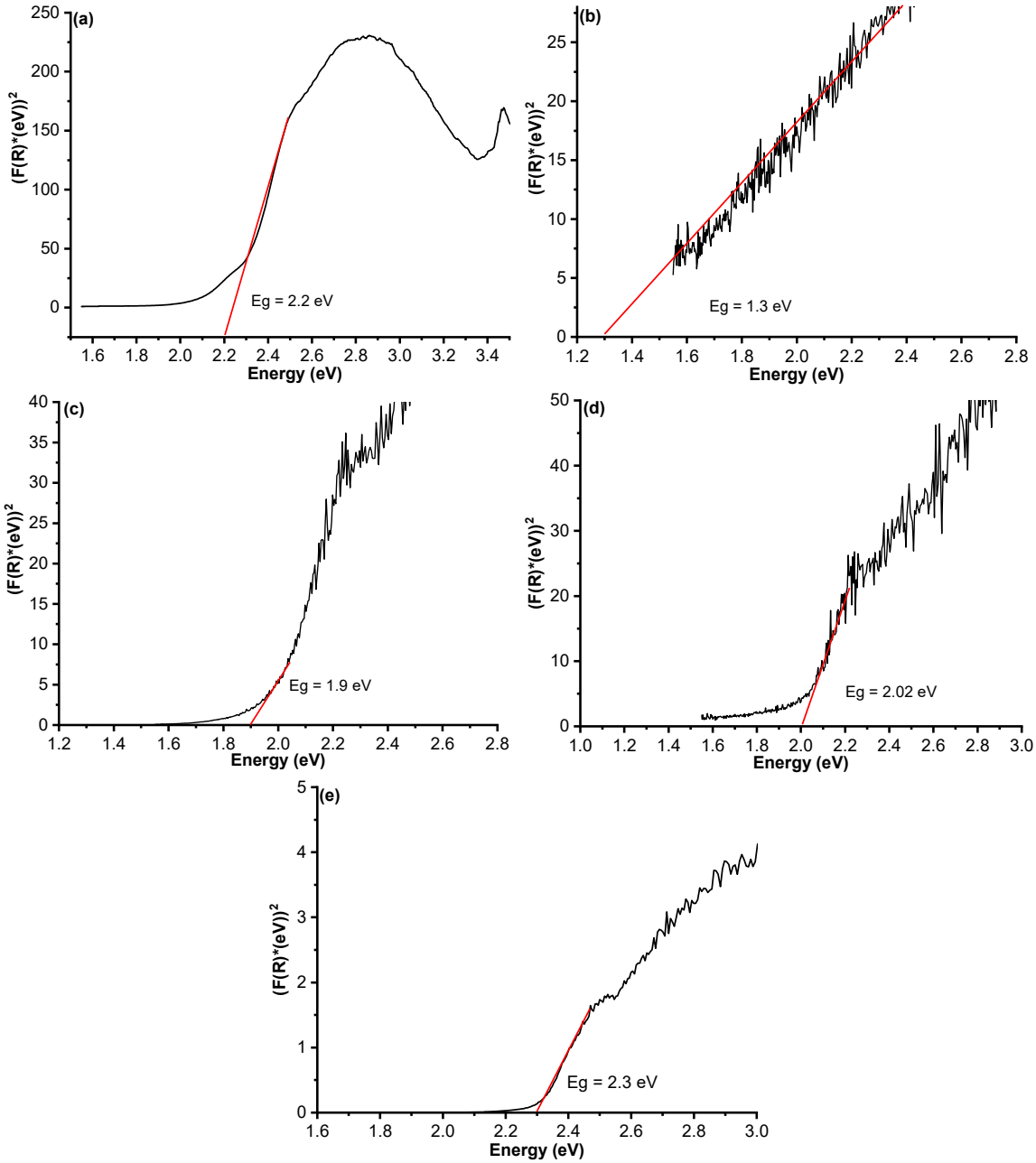

Fig 3. Band gap energy curves derived from UV-Vis diffuse reflectance spectroscopy (DRS) spectra for (A) MOF La-PTC; (B) $Ti_3C_2T_x$ MXene; (C) La-PTC-HIna; (D) La-PTC-HIna/$Ti_3C_2T_x$ MXene, and (E) La-PTC/$Ti_3C_2T_x$ MXene

The measured parameters of those five materials include the specific surface area (S_{BET}), the total pore volume (V_p), and the average pore size (D_p). Modulated isonicotinic acid (HIna) improved the surface area, pore volume, and pore size of La-PTC (Table 3). Table 3 exhibited that all materials have pore size distribution found in the 2–25 nm range. It is assumed that they were mesoporous materials groups, which have the advantage of being a photocatalyst that can provide a short distance to reduce the recombination of photo-excited electron and hole pairs [25]. Modulated isonicotinic acid (HIna) and loading of $Ti_3C_2T_x$ MXene on the MOF La-PTC do not destroy the MOF's mesoporosity.

The morphological features of all materials were determined by scanning electron microscopy (SEM). Fig. 4(a) shows the multilayer nanoflakes of $Ti_3C_2T_x$

MXene. It was produced when Ti_3AlC_2 released H_2 gas during the exothermic reaction of HF and the process of freeze-drying [26]. Fig. 4(b) shows that the La-PTC has a rod shape structure with various lengths and diameters. The structure of La-PTC has a good homogeneity, as indicated by the crystal structure having almost the same morphology at each observation point.

The EDS characterization in Table 4 exhibited that La-PTC/$Ti_3C_2T_x$ MXene and La-PTC/$Ti_3C_2T_x$ MXene contain elements derived from their constituents, namely $Ti_3C_2T_x$ MXene, La-PTC and La-PTC-HIna. It confirmed that combining the two compounds has succeeded in producing hybrid compounds that are different from their constituent precursors.

Table 3. Surface area, pore volume, and pore size of materials

Material	S_{BET} ($m^2\ g^{-1}$)	V_p ($cm^3\ g^{-1}$)	D_p (nm)
$Ti_3C_2T_x$ MXene	2.0892	0.0127	24.3011
La-PTC	22.2364	0.0685	12.3291
La-PTC-HIna	55.3904	0.1927	13.9166
La-PTC/$Ti_3C_2T_x$ MXene	34.8508	0.1033	11.8532
La-PTC-HIna/$Ti_3C_2T_x$ MXene	43.2119	0.1655	15.3235

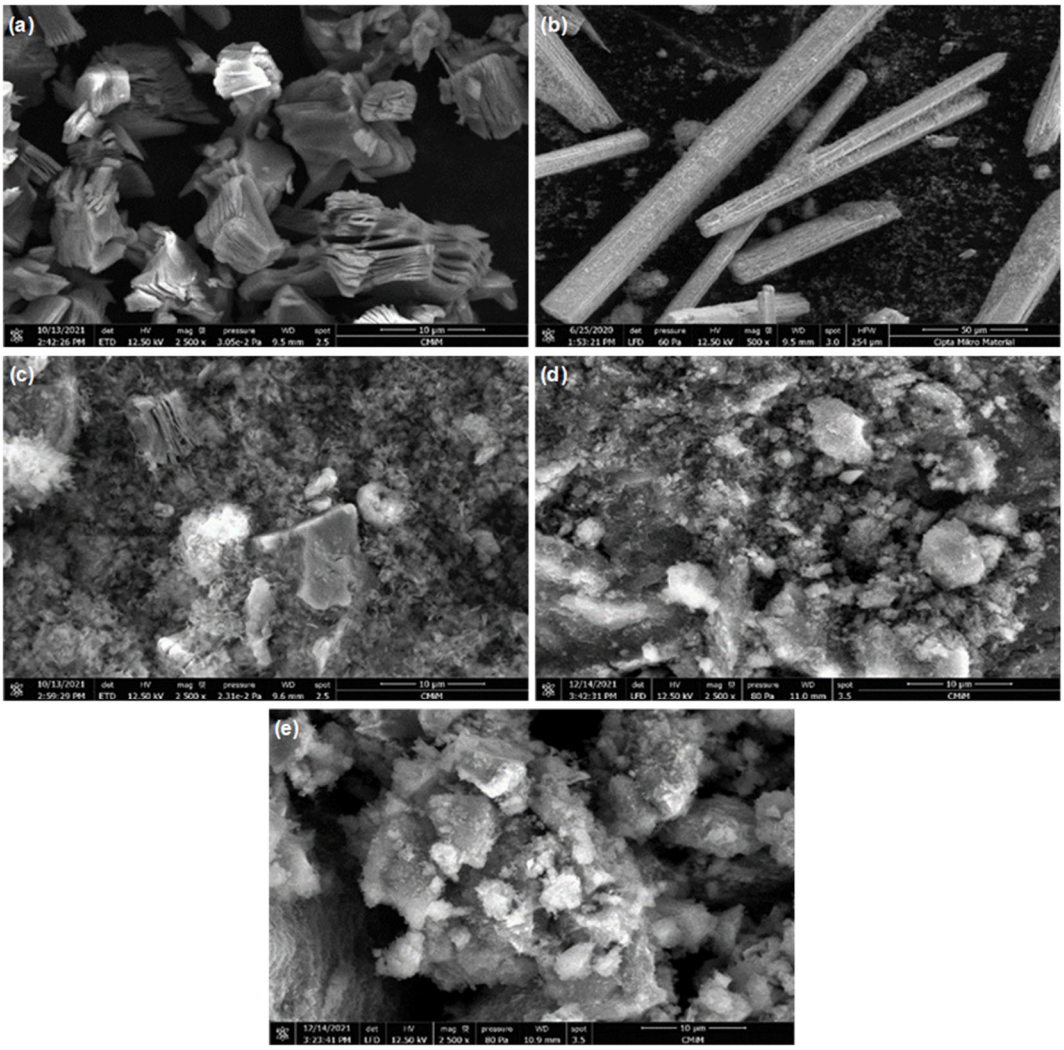

Fig 4. Scanning electron microscope (SEM) morphology of (a) $Ti_3C_2T_x$ MXene; (b) La-PTC; (c) La-PTC/$Ti_3C_2T_x$ MXene; (d) La-PTC-HIna; (e) La-PTC-HIna/$Ti_3C_2T_x$ MXene

Table 4. Element composition of materials

Element	Material				
	$Ti_3C_2T_x$ MXene	La-PTC	La-PTC-HIna	La-PTC/$Ti_3C_2T_x$ MXene	La-PTC-HIna/$Ti_3C_2T_x$ MXene
C	17.44	51.8	54.61	51.30	29.15
O	14.97	28.3	12.07	19.69	12.07
F	14.81			2.29	13.08
Al	1.26		4.41	0.34	0.94
Ti	51.52			9.35	19.78
La		19.9	23.97	17.05	24.27

Degradation of Methylene Blue

Fig. 5 shows the methylene blue degradation efficiency by La-PTC, $Ti_3C_2T_x$ MXene, La-PTC/$Ti_3C_2T_x$ MXene, La-PTC-HIna, and La-PTC-HIna/$Ti_3C_2T_x$ MXene for 210 min time reaction. Methylene blue degradation can be attained in dark and light conditions and occurs through surface adsorption and photocatalytic degradation mechanisms. Fig. 5 observed that La-PTC and La-PTC/$Ti_3C_2T_x$ MXene have no photocatalytic activity. Zulys et al. [9] explained that the photocatalytic activity of La-PTC depends on the electron-hole recombination process. The conduction band (CB) of La-PTC (-1.60 eV) which less negative than the lowest unoccupied molecular orbital (LUMO) of methylene blue (-0.25 eV), and the valence band (VB) of La-PTC (+0.61 eV) is less positive than highest occupied molecular orbital (HOMO) of MB (+1.66 eV). Thus, photoexcited electron-hole pairs do not oxidize the MB to produce the MB radical (MB•). Then it will be recombined, and the formation of radical species was not produced. Therefore, it inhibited the methylene blue photocatalytic degradation. On the other hand, the degradation efficiency of methylene blue by $Ti_3C_2T_x$ MXene, La-PTC-HIna, and La-PTC-HIna/Ti_3C_2 MXene hybrid in the light condition was higher than in dark conditions. It confirmed that those materials have the photocatalytic activity to degrade methylene blue.

In dark conditions, $Ti_3C_2T_x$ MXene degrades methylene blue through an adsorption mechanism that was influenced by electrostatic interaction between the negative charge of both hydroxyl (-OH) and fluoride (F^-) termination group on the $Ti_3C_2T_x$ MXene surface and positive charge on sulfur (S) or nitrogen (N) on the methylene blue molecule [27]. These F^- and OH termination groups are developed to form negative charges on the $Ti_3C_2T_x$ MXene surface, such as $[Ti\text{-}F]^-$

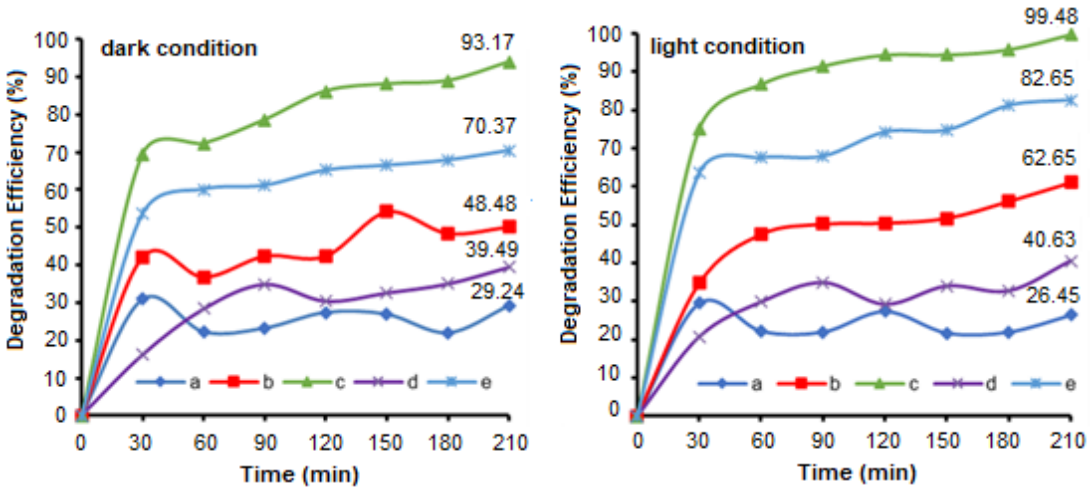

Fig 5. Degradation efficiency of methylene blue for different materials: (a) La-PTC, (b) $Ti_3C_2T_x$ MXene, (c) La-PTC-HIna, (d) La-PTC/$Ti_3C_2T_x$ MXene, and (e) La-PTC-HIna/$Ti_3C_2T_x$ MXene in the dark and light irradiation

and $[TiO]^-H^+$, which are acted as receptors to cationic species such as methylene blue [27]. The complex formation between methylene blue and $Ti_3C_2T_x$ MXene is given below.

$[Ti\text{-}F]^- + MB \rightarrow Ti\text{-}F\text{-}MB$ (1)

$[Ti\text{-}O]^-H^+ \rightarrow [Ti\text{-}O]^- + H^+$ (2)

$[Ti\text{-}O]^- + MB \rightarrow Ti\text{-}O\text{-}MB$ (1)

My Tran et al. [27] explained that the F^- terminated group on MXene plays a prominent role in the adsorption of MB. The adsorption capability of $Ti_3C_2T_x$ MXene on methylene blue decreased as the pH increased from 2 to 7 [27]. Increasing the pH causes a decrease in the number of F^- termination groups on the surface of the $Ti_3C_2T_x$ MXene because F^- terminated groups were replaced with OH^- ions from water. It also, the electronegativity of F is larger than O ($\chi F = 3.98$, $\chi O = 3.44$), leading to the remarkable ability of most F^- terminated $Ti_3C_2T_x$ to attract and absorb MB species. In addition, after the F^- group is replaced with an OH^- group, the degree of electrostatic attraction between O^- and MB^+ decreases with H^+ compensation [27]. Lim et al. [28] reported that increasing the pH solution explained the increase in the adsorption capacity of $Ti_3C_2T_x$ MXene to methylene blue. At the high pH level, $Ti_3C_2T_x$ MXene was more negatively charged. It is attributed to promoting the adsorption of cationic dyes like methylene blue via electrostatic attraction. Otherwise, the $Ti_3C_2T_x$ MXene surface becomes a relatively less negative charge at a low pH level because the hydroxyl group (OH^-) is neutralized on the $Ti_3C_2T_x$ MXene surface by hydrogen ion (H^+) in solution.

Hasan and Jhung [29] explained that the MB adsorption by MOF occurred through electrostatic, hydrophobic, acid-base, π-π, hydrogen attraction, or a combination of these interactions. In La-PTC, the electrostatic attraction occurs between the positive charge of MB and the negative charge of MOF La-PTC. π-π interaction occurred through π bonding in the aromatic ring in MB and the aromatic ring in the perylene linker contained in the La-PTC. The hydrogen attraction was constructed between the hydrogen of MB and the oxygen of perylene. In addition, the hydrogen interaction between hydrogen in MB and nitrogen from the pyridine ring of isonicotinic acid contributed to La-PTC-HIna.

Fig. 5 shows that under dark conditions, the five materials' adsorption ability is affected by their surface area, volume, and pore size. La-PTC-HIna has the highest adsorption ability, producing a degradation efficiency of 93.95% compared to the other four materials. It is because La-PTC-HIna has the highest surface area, pore volume, and pore size (except $Ti_3C_2T_x$ MXene and La-PTC-HIna/$Ti_3C_2T_x$ MXene pore size), which is 55.3904 m^2/g, 0.1927 cm^3/g and 13.9166 nm (Table 2). Although $Ti_3C_2T_x$ MXene has a lower surface area and pore volume than La-PTC and La-PTC/$Ti_3C_2T_x$ MXene, it has a higher adsorption capacity (48.48%) due to its pore size, which is twice the pore size of La-PTC and La-PTC/$Ti_3C_2T_x$ MXene (Table 2). The same thing was also proven by Gupta et al. [30], who succeeded in synthesizing Cu-BTC, Ag-Cu-BTC, and Ca-Cu-BTC with a surface area of 163.43, 187.64, and 17.08 m^2/g, respectively. The total pore volume is 0.144, 0.113, and 0.299 cm^3/g, and the pore size is 3.5, 2.4, and 70.1 nm. The adsorption activity of MOFs Cu-BTC, Ag-Cu-BTC, and Ca-Cu-BTC against methylene blue compounds was 12.7, 8.9, and 19.6 mg/g.

Fig. 5 also exhibits that under light irradiation, MOF La-PTC-HIna has the highest photocatalytic activity among other materials, with a degradation efficiency of 99.48%. The addition of isonicotinic acid as a modulator enhanced the photocatalytic activity of La-PTC. The isonicotinic acid in the La-PTC-HIna acts as a linker competitor. It competes with perylene to replace some of the perylene ligands in the La-PTC [31]. The perylene replacement by the isonicotinic acid formed a MOF with a smaller particle size [20]. The smaller particle size of the MOFs increases the surface area of MOFs. Therefore, the pores containing the active site will increase [32]. It generates an increasing number of active sites, and the photocatalytic activity will be higher.

■ CONCLUSION

La-PTC, $Ti_3C_2T_x$ MXene, La-PTC-HIna, La-PTC/$Ti_3C_2T_x$ MXene, and La-PTC-HIna/$Ti_3C_2T_x$ MXene were comparatively evaluated for their application as photocatalysts in the methylene blue degradation. La-PTC-HIna has the most significant degradation activity compared to La-PTC, $Ti_3C_2T_x$

MXene, La-PTC/$Ti_3C_2T_x$ MXene, and La-PTC-HIna/$Ti_3C_2T_x$ MXene hybrid with a degradation efficiency of 99.48% in 20 ppm methylene blue under visible irradiation for 210 min. The degradation of methylene blue by La-PTC-HIna occurs via the adsorption and photocatalytic mechanism. The methylene blue degradation by La-PTC-HIna/$Ti_3C_2T_x$ MXene hybrid is lower than La-PTC-HIna due to a decrease in surface area and pore volume in the material after the loading of $Ti_3C_2T_x$ MXene.

■ ACKNOWLEDGMENTS

The authors wish to thank the PUTI UI Research Grant for financial support in carrying out this work through the research contract number NKB-1940/UN2.RST/HKP.05.00/2020.

■ REFERENCES

[1] Saeed, M., Usman, M., and ul Haq, A., 2018, "Catalytic Degradation of Organic Dyes in Aqueous Medium" in *Photochemistry and Photophysics – Fundamentals to Applications*, Eds. Saha, S., and Mundal, S., IntechOpen, Rijeka, Croatia, 197–211.

[2] Khelifi, S., and Ayari, F., 2019, Modified bentonite for anionic dye removal from aqueous solutions. Adsorbent regeneration by the photo-Fenton process, *C. R. Chim.*, 22 (2-3), 154–160.

[3] Saini, J., Garg, V.K., Gupta, R.K., and Kataria, N., 2017, Removal of Orange G and Rhodamine B dyes from aqueous system using hydrothermally synthesized zinc oxide loaded activated carbon (ZnO-AC), *J. Environ. Chem. Eng.*, 5 (1), 884–892.

[4] Fan, Y.H., Zhang, S.W., Qin, S.B., Li, X.S., and Qi, S.H., 2018, An enhanced adsorption of organic dyes onto NH_2 functionalization titanium-based metal-organic frameworks and the mechanism investigation, *Microporous Mesoporous Mater.*, 263, 120–127.

[5] Ibrahim, Y., Meslam, M., Eid, K., Salah, B., Abdullah, A.M., Ozoemena, K.I., Elzatahry, A., Sharaf, M.A., and Sillanpa, M., 2022, A review of MXenes as emergent materials for dye removal from wastewater, *Sep. Purif. Technol.*, 282, 120083.

[6] Lu, W., Wei, Z., Gu, Z.Y., Liu, T.F., Park, J., Park, J., Tian, J., Zhang, M., Zhang, Q., Gentle III, T., Bosch, M., and Zhou, H.C., 2014, Tuning the structure and function of metalorganic frameworks via linker design, *Chem. Soc. Rev.*, 43 (16), 5561–5593.

[7] Alqadami, A.A., Naushad, M., Alothman, Z.A., and Ahamad, T., 2018, Adsorptive performance of MOF nanocomposite for methylene blue and malachite green dyes: Kinetics, isotherm and mechanism, *J. Environ. Manage.*, 223, 29–36.

[8] Gong, X., Zhao, R., Qin, J., Wang, H., and Wang, D., 2019, Ultra-efficient removal of NO in a MOFs-NTP synergistic process at ambient temperature, *Chem. Eng. J.*, 358, 291–298.

[9] Zulys, A., Adawiah, A., Gunlazuardi, J., and Yudhi, M.D.L., 2021, Light-harvesting metal-organic frameworks (MOFs) La-PTC for photocatalytic dyes degradation, *Bull. Chem. React. Eng. Catal.*, 16 (1), 170–178.

[10] Zhang, F.H., Wang, Y.Y., Lv, C., Li, Y.C., and Zhao, X.Q., 2019, Luminescent complexes associated with isonicotinic acid, *J. Lumin.*, 207, 561–570.

[11] Garibay, S.J., Iordanov, I., Islamoglu, T., DeCoste, J.B., and Farha, O.K., 2018, Synthesis and functionalization of phase-pure NU-901 for enhanced CO_2 adsorption: The influence of zirconium salt and modulator on topology and phase purity, *CrystEngComm*, 20 (44), 7066–7070.

[12] Adawiah, A., Oktavia, W., Saridewi, N., Azhar, F.M., Fitria, R.N., Gunawan, M.S., Komala, S., and Zulys A., 2022, Synthesis metal-organic framework (MOFs) Cr-PTC-HIna modulated isonicotinic acid for methylene blue photocatalytic degradation, *Bull. Chem. React. Eng. Catal.*, 17 (2), 383–393.

[13] Wang, H., Zhao, R., Qin, J., Hu, H., Fan, X., Cao, X., and Wang, D., 2019, MIL-100(Fe)/Ti_3C_2 MXene as a Schottky catalyst with enhanced photocatalytic oxidation for nitrogen fixation activities, *ACS Appl. Mater. Interfaces*, 11 (47), 44249–44262.

[14] Anasori, B., Xie, Y., Beidaghi, M., Lu, J., Hosler, B.C., Hultman, L., Kent, P.R.C., Gogotsi, Y., and Barsoum, M.W., 2015, Two-dimensional, ordered, double transition metals carbides (MXenes), *ACS Nano*, 9 (10), 9507–9516.

[15] Khazaei, M., Arai, M., Sasaki, T., Chung, C.Y., Venkataramanan, N.S., Estili, M., Sakka, Y., and Kawazoe, Y., 2013, Novel electronic and magnetic properties of two-dimensional transition metal carbides and nitrides, *Adv. Funct. Mater.*, 23 (17), 2185–2192.

[16] Naguib, M., Mochalin, V.N., Barsoum, M.W., and Gogotsi, Y., 2014, MXenes: A new family of two-dimensional materials, *Adv. Mater.*, 26 (7), 992–1005.

[17] Khazaei, M., Arai, M., Sasaki, T., Estili, M., and Sakka, Y., 2014, Two-dimensional molybdenum carbides, potential thermoelectric materials of the MXene family, *Phys. Chem. Chem. Phys.*, 16 (17), 7841–7849.

[18] Jun, B.M., Kim, S., Heo, J., Park, C.M., Her, N., Jang, M., Huang, Y., Han, J., and Yoon, Y., 2018, Review of MXenes as new nanomaterials for energy storage/delivery and selected environmental applications, *Nano Res.*, 12 (3), 471–487.

[19] Khazaei, M., Ranjbar, A., Arai, M., Sasaki, T., and Yunoki, S., 2017, Electronic properties and applications of MXenes: A theoretical review, *J. Mater. Chem. C*, 5 (10), 2488–2503.

[20] Wang, F., Guo, H., Chai, Y., Li, Y., and Liu, C., 2013, The controlled regulation of morphology and size of HKUST-1 by "coordination modulation method", *Microporous Mesoporous Mater.*, 173, 181–188.

[21] Tian, P., He, X., Zhao, L., Li, W., Fang, W., Chen, H., Zhang, F., Huang, Z., and Wang, H., 2019, Enhanced charge transfer for efficient photocatalytic H_2 evolution over UiO-66-NH_2 with annealed $Ti_3C_2T_x$ MXenes, *Int. J. Hydrogen Energy*, 44 (2), 788–800.

[22] Zhao, X., Liu, M., Chen, Y., Hou, B., Zhang, N., Chen, B., Yang, N., Chen, K., Li, J., and An, L., 2015, Fabrication of layered Ti_3C_2 with an accordion-like structure as a potential cathode material for high performance lithium-sulfur batteries, *J. Mater. Chem. A*, 3 (15), 7870–7876.

[23] Mu, X., Jiang, J., Chao, F., Lou, Y., and Chen, J., 2018, Ligand modification of UiO-66 with an unusual visible light photocatalytic behavior for RhB degradation, *Dalton Trans.*, 47 (6), 1895–1902.

[24] Lukatskaya, M.R., Mashtalir, O., Ren, C.E., Dall'Agnese, Y., Rozier, P., Taberna, P.L., Naguib, M., Simon, P., Barsoum, M.W., and Gogotsi, Y., 2013, Cation intercalation and high volumetric capacitance of two-dimensional titanium carbide, *Science*, 341 (6153), 1502–1505.

[25] Chang, S.S., Clair, B., Ruelle, J., Beauchêne, J., Di Renzo, F., Quignard, F., Zhao, G.J., Yamamoto, H., and Gril, J., 2009, Mesoporosity as a new parameter for understanding tension stress generation in trees, *J. Exp. Bot.*, 60 (11), 3023–3030.

[26] Alhabeb, M., Maleski, K., Anasori, B., Lelyukh, P., Clark, L., Sin, S., and Gogotsi, Y., 2017, Guidelines for synthesis and processing of two-dimensional titanium carbide ($Ti_3C_2T_x$ MXene), *Chem. Mater.*, 29 (18), 7633–7644.

[27] My Tran, N., Thanh Hoai Ta, Q., Sreedhar, A., and Noh. J.S., 2021, $Ti_3C_2T_x$ MXene playing as a strong methylene blue adsorbent in wastewater, *Appl. Surf. Sci.*, 537, 148006.

[28] Lim, S., Kim, J.H., Park, H., Kwak, C., Yang, J., Kim, J., Ryu, S.Y., and Lee, J., 2021, Role of electrostatic interactions in the adsorption of dye molecules by Ti_3C_2-MXenes, *RSC Adv.*, 11 (11), 6201–6211.

[29] Hasan, Z., and Jhung, S.H., 2015, Removal of hazardous organics from water using metal-organic frameworks (MOFs): Plausible mechanisms for selective adsorptions, *J. Hazard. Mater.*, 283, 329–339.

[30] Gupta, N.K., Bae, J., and Kim, K.S., 2022, Role of bimetallic solution in the growth and functionality of Cu-BTC metal-organic framework, *Materials*, 15 (8), 2804.

[31] Hasan, M.R., 2015, Pengaruh Penambahan Modulator Asam Asetat pada Sintesis Metal Organic Framework Tipe HKUST-1, *Undergraduate Thesis*, Intitute Teknologi Sepuluh Nopember, Surabaya, Indonesia.

[32] Tambun, R., Limbong, H.P., Pinem, C., and Manurung, E., 2016, Pengaruh ukuran partikel, waktu dan suhu pada ekstraksi fenol dari lengkuas merah, *Jurnal Teknik Kimia USU*, 5 (4), 53–56.